CHAPTER EIGHT

Electrocatalytic Properties of Prussian Blue Nanoparticles Supported on Poly(m-Aminobenzenesulfonic Acid) – Funtionalized Single-Walled Carbon Nanotubes Towards the Detection of Dopamine*

* The publication below resulted from part of the research work presented in this chapter and it is not referenced further in this thesis:

9. **Abolanle S. Adekunle**, Jeseelan Pillay, Kenneth I. Ozoemena, (Submitted)

8.1 Comparative TEM and AFM images and UV-vis spectra

Figure 8.1 showed the transmission electron (TEM) micrographs and size distributions for the PB (a) and the SWCNT-PB (b) nanocomposite material. The PB nanoparticles appear a little amorphous and distribute uniformly across the SWCNT-PABS due to the strong electrostatic interaction between the functionalised SWCNT-PABS and the PB nanoparticles. There is an electrostatic interaction between the hydrophilic ends (SO_3^{2-}) of the SWCNT-PABS and the Fe^{3+} cations from $FeCl_3$ which eventually leads to the permeation and adsorption of the Fe^{3+} ions into the interlayer of the SWCNT-PABS. XPS study had also shown that Fe^{3+} was successfully adsorbed on the surface of MWCNTs [1] The adsorbed Fe^{3+} reacts with the $[Fe(CN)_6]^{4-}$ anion from $K_4[Fe(CN)_6]$ forming non-stoichiometric deposits of $Fe_x[Fe(CN)_6]_y$ on the interlayer of the SWCNT-PABS. Since the precipitation is non-stoichiometric, there are more active sites of C=N groups with which more Fe^{3+} ions can react for further PB deposition from several deposition cycles. For the GC-PB, the mechanism may be described as a physical adsorption of the Fe^{3+} on the electrode which later react with the Fe^{2+} from $[Fe(CN)_6]^{4-}$ to form PB nanoparticles. The PB nanoparticle sizes are in the 50 – 500 nm range. The particle sizes are much lower as obtained from the AFM analysis.

The AFM results (Figure 8.1c and 8.1d) clearly showed the successful deposition of PB nano particles on the GC plate. The topographic image of the GC-SWCNT-PB gave a particle size dimension in the nano range of about 90 nm (Figure 8.1c) while the cross-sectional size diameter is in the range of 11-18 nm compared with the bare-GC and the GC-SWCNT-PABS (not shown) with particle size diameters of about 2 and 10 nm respectively, indicating

successful deposition of PB nanoparticles. GC plate was used as substitute for EPPGE in obtaining this result since it fits conveniently into the equipment.

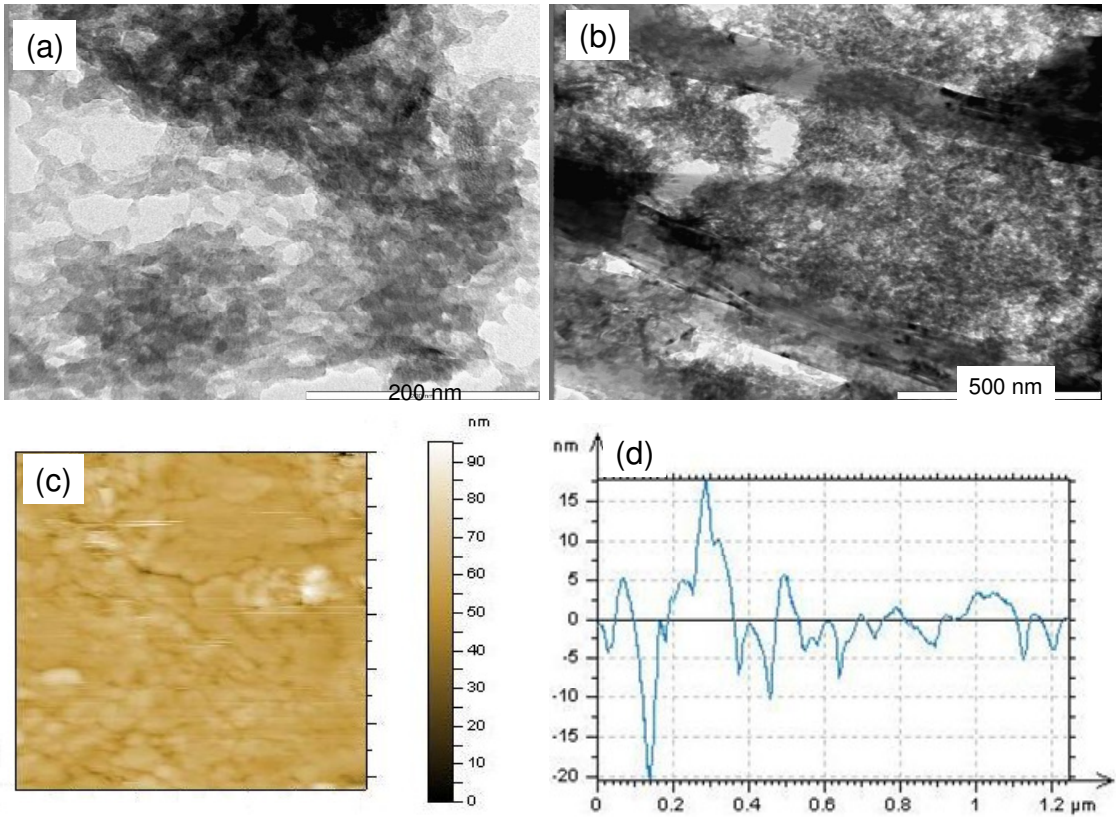

Figure 8.1: Typical TEM images of (a) PB and (b) SWCNT-PB nanoparticles. (c) and (d) are the AFM topography image and the cross section of the SWCNT-PB showing the particle size distribution in nano dimensions.

8.1.1. UV-vis-absorption spectroscopy characterization of the SWCNT-PABS, PB and the SWCNT-PB nanoparticles.

UV-vis absorption spectroscopy experiment was performed to further prove the deposition of PB on the SWCNT-PABS. The thin solid PB film deposited on the electrode was washed with distilled water and made into solution for UV-vis analysis. Figure 8.2

compares the UV-vis spectra of the PB, SWCNT-PABS and the SWCNT-PB film formed on the electrode after deposition. The SWCNT-PABS have a characteristic absorption band at about 243 nm which is lower than the 260 nm reported by Wang et al. [2] and described previously by authors as the characteristic of the adsorption of the assembled CNTs [3]. The difference can be attributed to the smooth and the pure nature of the SWCNT-PABS, with the absence of other light absorbing groups that may lead to an increase absorption band. The PB have a characteristic absorption band at around 667 nm, corresponding to the mixed-valence charge-transfer absorbance of the [Fe(II)-C-N-Fe(III)] complex. This result agreed with literature values [1,2]. The absorption bands at 243 nm for the SWCNT-PABS disappeared after the deposition of PB nanoparticles on the SWCNT-PABS to give SWCNT-PB nanoparticles indicating successful transformation of the SWCNT-PABS to SWCNT-PB.

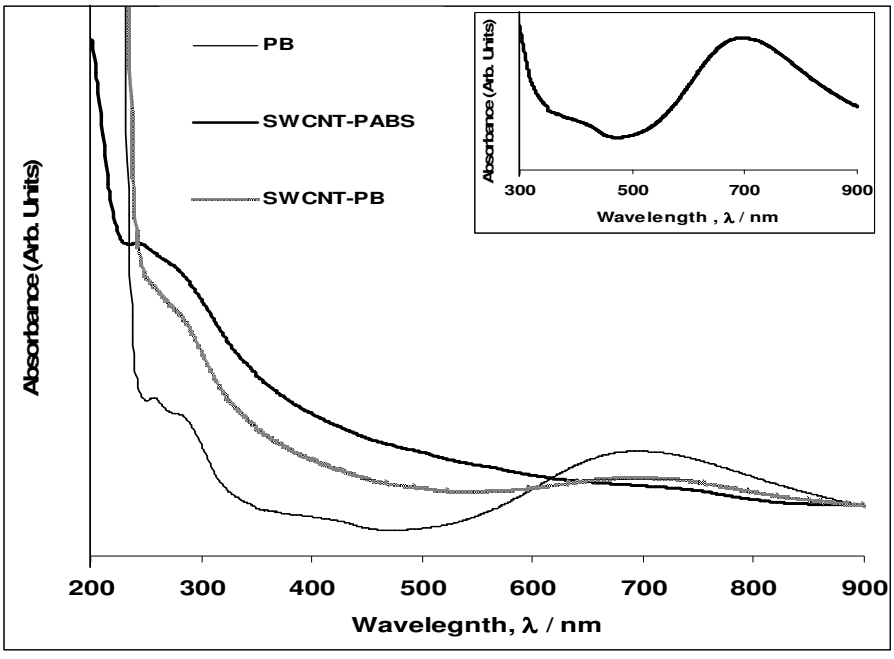

Figure 8.2: UV/VIS spectra of Prussian blue (PB), SWCNT-PABS and SWCNT-PB.

8.2. Cyclic voltammetric characterisation of the electrodes.

Figure 8.3a represents the cyclic voltammograms obtained for the EPPGE (i), EPPGE-SWCNTPABS (ii), and EPPGE-SWCNTPABS-PB (iii) in pH 7.0 PBS containing 0.1 M KCl (scan rate: 25 mVs^{-1}). The broad redox couple at around 0.5 – 0.8 V prominent at the bare EPPGE and SWCNTPABS is related to the redox processes arising from the oxo-containing species existing at the edge plane sites of these species. Unlike the bare EPPGE and EPPGE-SWCNTPABS, the EPPGE-SWCNTPABS-PB showed well defined redox peaks: anodic peak at 0.25 V due to PB, reduction peak at 0.1 V due to the Prussian white (PW), and a very weak anodic peak at ~0.9 V due to the Prussian yellow (PY) [4]. These signature peaks confirm the successful integration of the PB onto the SWCNTPABS structure. These characteristic peaks of the PB were best observed when higher concentration of the PB (i.e., EPPGE-SWCNTPABS-3PB) is integrated onto the SWCNTPABS (see Figure 8.3b). As evident in Figure 8.3b, the EPPGE-SWCNT-3PB film showed little or no drop in current density when the electrode was subjected to continuous cycling (50 scans) in the electrolyte, which is a clear indication of excellent electrochemical stability. In addition, the broad peak at around 0.5-0.8 V (of the oxo-containing species) disappeared, suggesting the replacement or covering of these oxo-species with the PB nanoparticles. The different redox processes observed at the PB modified electrodes can be summarised by the Equations (8.1 and 8.2) below [4]:

$$KFe(III)[Fe(II)(CN)_6] - e^- - K^+ \longrightarrow Fe(III)[Fe(III)(CN)_6] \quad (8.1)$$

PB PY

$$KFe(III)[Fe(II)(CN)_6] + e^- + K^+ \longrightarrow K_2Fe(II)[Fe(II)(CN)_6] \quad (8.2)$$

PB PW)

The surface coverage of the electroactive PB films (Γ_{PB}) on the EPPGE-SWCNT-3PB electrode was estimated using Equation 8.3 below:[5]

$$\Gamma_{PB} = \frac{Q}{nFA} \quad (8.3)$$

where *Q* is the quantity of charge obtained by integration of the area under the anodic PB peak, *n* is number of electron transfer during the process, *F* is the Faraday constant, and *A* is the geometric area of the working electrode. The Γ_{PB} is approximately 4.8 x 10^{-8} mol cm^{-2}.

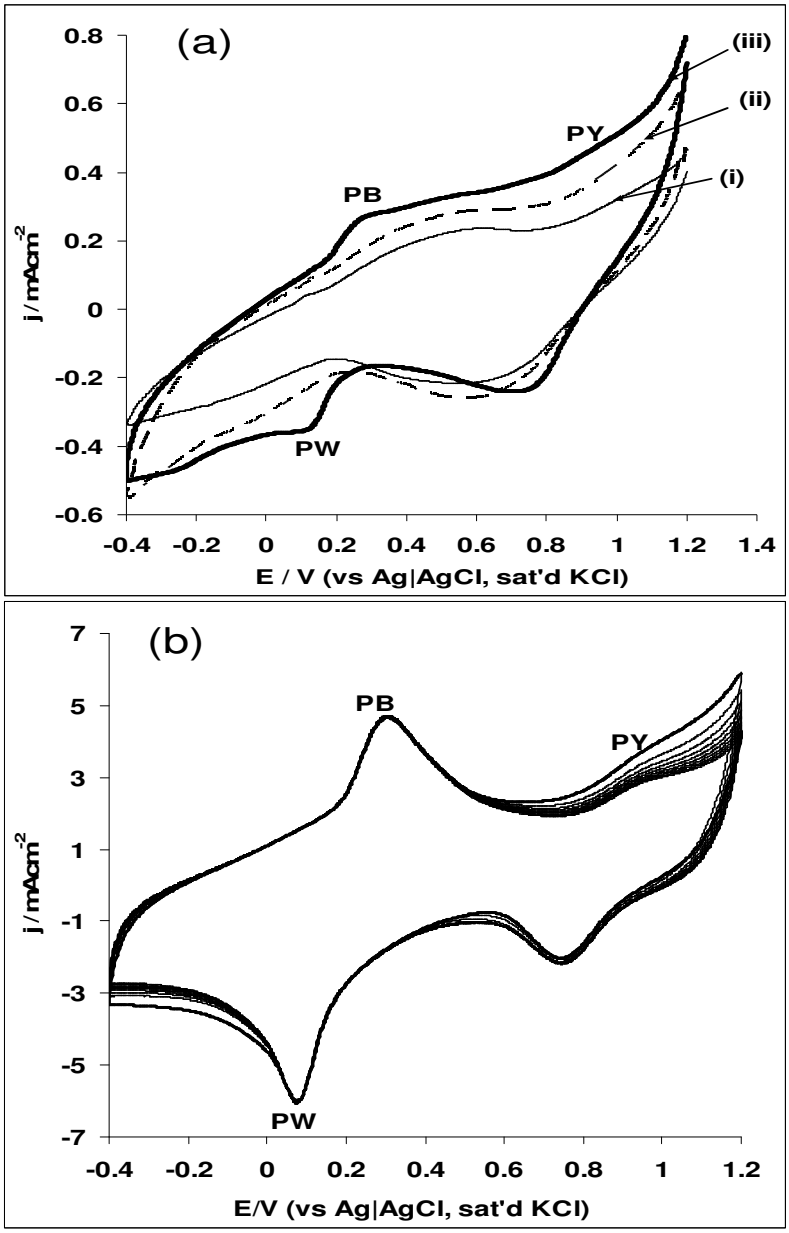

Figure 8.3: Typical cyclic voltammograms of (a) EPPGE (i), EPPGE-SWCNT-PABS (ii) and EPPGE-SWCNT-PB (iii) in 0.1 M KCl electrolyte (scan rate: 25 mVs^{-1}). (b) is the cyclic voltammogram showing the electrochemical stability of EPPGE–SWCNT-3PB modified electrode (50 cycles) in pH 7.0 PBS containing 0.1 M KCl electrolytes (scan rate: 100 mVs^{-1}).

8.3. Electrocatalytic oxidation of dopamine

Figure 8.4a compares the cyclic voltammograms (after background current subtraction) of the electrodes in pH 7.0 PBS containing $2x10^{-4}$ M dopamine. The current density follows the order: EPPGE-SWCNTPABS-PB (~ 617.0 μAcm^{-2}) > EPPGE-SWCNTPABS (~ 301.0 μAcm^{-2}) > bare-EPPGE (~ 124.0 μAcm^{-2}) > EPPGE-PB (~ 140.0 μAcm^{-2}). In addition, DA catalysis was much favoured at EPPGE-SWCNTPABS-PB in terms of low onset (~0.04 V) as well as anodic peak potential (E_{pa} ≈ 0.279 V) compared to other electrodes that show higher values. Similar experiment was performed using CTAB/SWCNTPABS-PB electrodes where CTAB acts as PB stabilizer on the electrode. Contrary to expectation, the CTAB modified electrodes gave poor DA response compared with electrode without CTAB. EPPGE-SWCNTPABS-PB was identified as the best electrode for DA oxidation in this study, thus all subsequent studies were carried out with this electrode unless otherwise stated.

Next, the impact of different PB layers/concentrations as well as the concentrations of the $FeCl_3$ and $K_4[Fe(CN)_6]$ in the deposition solution on the electro-oxidation of DA (Figure 8.4b) was investigated. Three concentrations of $FeCl_3$ and $K_4[Fe(CN)_6]$ solutions (10^{-4}, 10^{-3} and 10^{-2} M) were used. Using the 10^{-4} M deposition solution, it was observed that as the PB layers increase the current response of the DA oxidation follow increases: 295.0 μAcm^{-2} (SWCNTPABS-3PB) > 257.0 μA (SWCNTPABS-2PB) > 146.0 μAcm^{-2} (SWCNTPABS-PB) (Figure 7.5b). Interestingly, using the different deposition solutions (10^{-4}, 10^{-3} and 10^{-2} M) to obtain the SWCNTPABS-3PB, the current rersponse for the DA remained essentially the same (295.0 μAcm^{-2}). This result suggests that at high concentration, the PB nanoparticles may form an insulating

layer thereby lowering DA catalysis. Han et al. [1] also observed similar situation and concluded that the low concentration of the deposition solution of PB would be preferred. Thus, it seems very reasonable and economical using low concentration (10^{-4} M) of $FeCl_3$ and $K_4[Fe(CN)_6]$ for the electrode modification with PB nanoparticles.

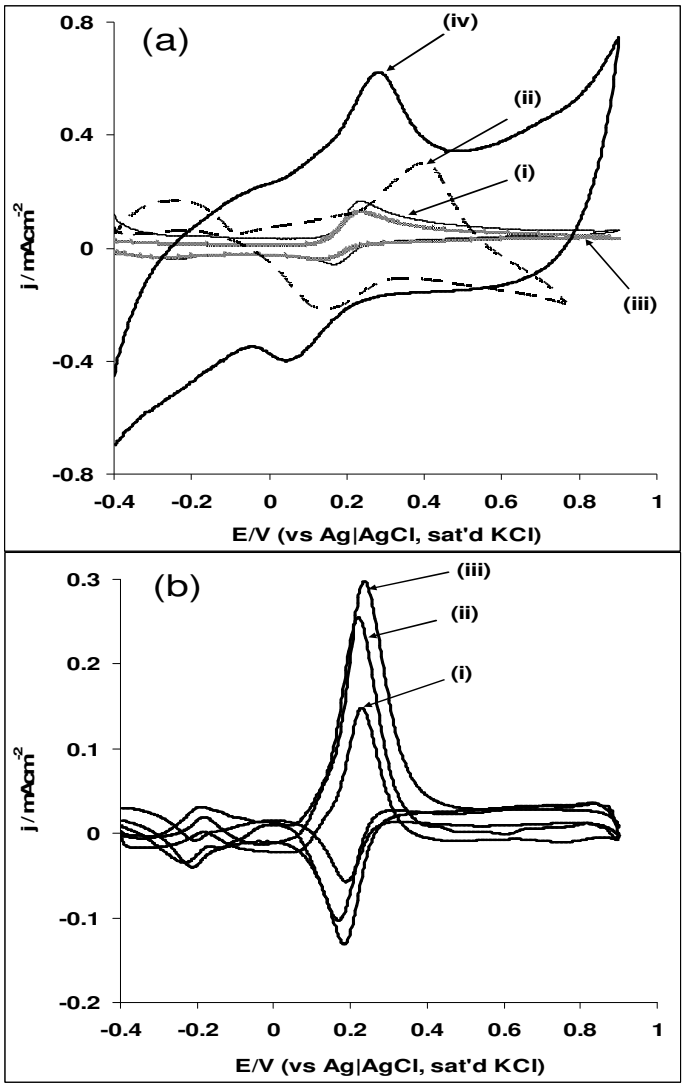

Figure 8.4: Cyclic voltammograms showing the current responses (background subtracted) of (a) (i) bare EPPGE, (ii) EPPGE-SWCNT-PABS, (iii) EPPGE-PB and (iv) EPPGE-SWCNT-PB in 0.1 M pH 7.0 PBS containing 2 x10^{-4} M DA (scan rate: 25 mVs^{-1}). (b) (i) EPPGE-SWCNT-PB, (ii) EPPGE-SWCNT-2PB and (iii) EPPGE-SWCNT-3PB in 0.1 M pH 7.0 PBS containing 2 x10^{-4} M DA (scan rate: 25 mVs^{-1}).

To examine the electron transfer behaviour of the three electrodes towards the oxidation of DA, electrochemical impedance spectroscopy (EIS) experiment was conducted in 2 x 10^{-4} M DA solution at the EPPEGE-SWCNTPABS-PB, EPPGE-SWCNTPABS-2PB and EPPGE-SWCNTPABS-3PB at a fixed potential of 0.2 V vs Ag|AgCl, sat'd KCl (Figure 8.5a). Figure 8.5a presents the Nyquist plots obtained and the circuit (inset) used to fit the spectra. The data obtained from the fittings are presented in Table 8.1, clearly showing satisfactory fitting as judged by the low chi-square function (χ^2) and relative errors. From Table 8.1, EPPGE-SWCNT-3PB electrode has the fastest electron transport. The R_{ct} values followed the order: EPPGE-SWCNTPABS-3PB (3.95 Ωcm^2) < EPPGE-SWCNTPABS-2PB (5.01 Ωcm^2) < EPPGE-SWCNTPABS-PB (5.33 Ωcm^2), indicating faster electron transfer towards DA electrocatalysis at the EPPGE-SWCNTPABS-3PB.

Bode plot of –phase angle vs. log (f/Hz) obtained for the different PB layers (Figure 8.5b) gave phase angles less than -90^o expected for an ideal capacitive behaviour. Also, the *n* values obtained (Table 8.1) are < 1.0, indicating the pseudocapacitive nature of the electrodes at every PB layer. Presently, there is little information on the electrochemical impedance study on DA oxidation.

Table 8.1: Impedance data obtained for the EPPGE-SWCNT-PB modified electrodes (at different deposition cycles) in 0.1M pH 7.0 PBS containing 2 x 10^{-4} M DA ($E_{1/2}$ = 0.2 V vs Ag|AgCl sat'd KCl).

EPPGE modifier	**Electrochemical Impedance Parameters**					
	R_s /Ωcm^2	**10^3 CPE/Fcm^{-2}**	**N**	**R_{ct} /Ωcm^2**	**10^3 Z_W/Ωcm^2**	**10^4 χ^2**
SWCNTPABS-PB	21.87±0.01	7.70±0.02	0.86±0.01	5.33±0.02	0.18±0.01	0.20
SWCNTPABS-2PB	19.66±0.01	7.10±0.04	0.87±0.01	5.01±0.04	0.15±0.01	2.37
SWCNTPABS-3PB	18.31±0.01	7.20±0.03	0.87±0.01	3.95±0.02	0.14±0.01	1.05

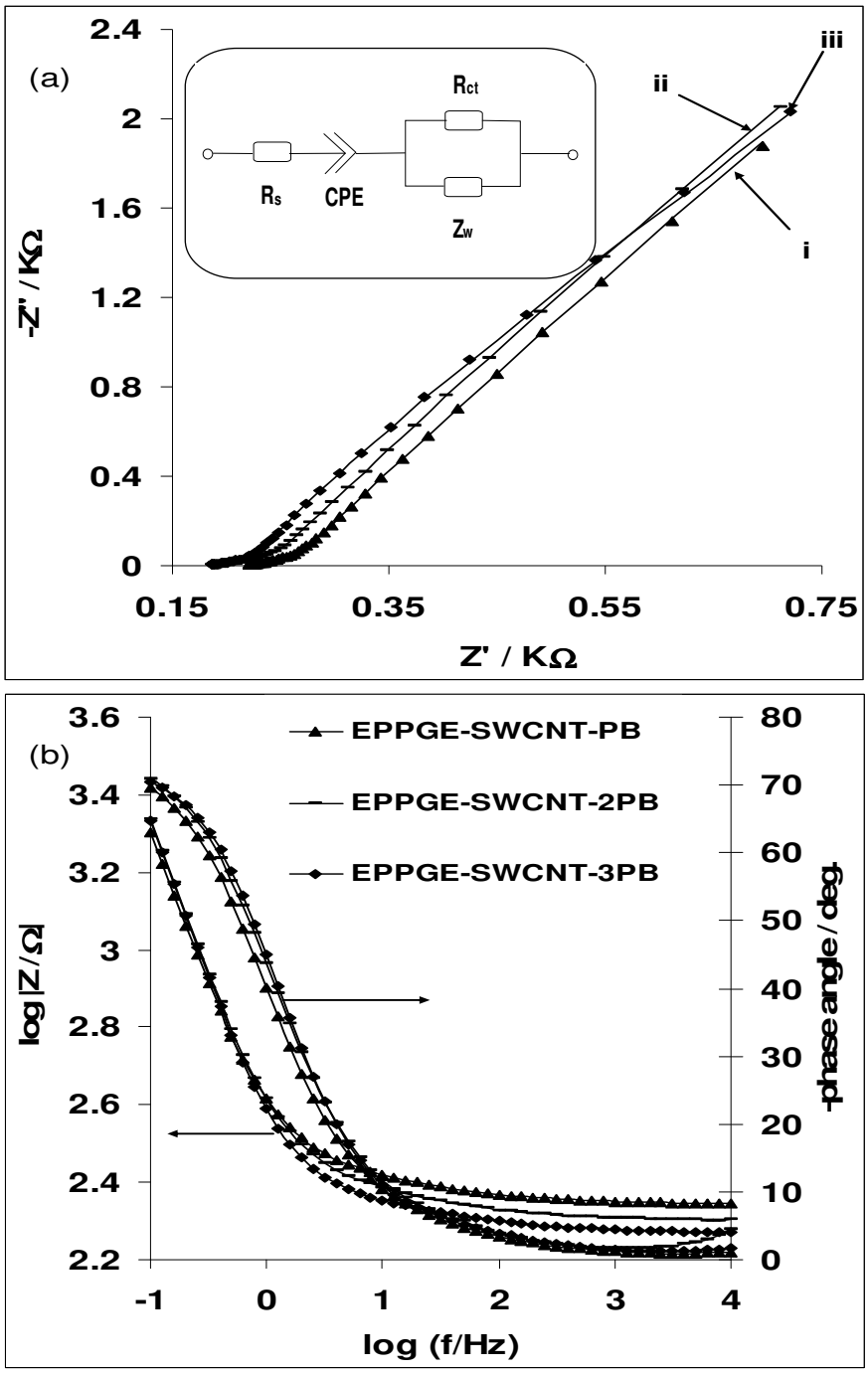

Figure 8.5: (a) Typical Nyquist plots obtained for (i) EPPGE-SWCNT-PB, (ii) EPPGE-SWCNT-2PB and (iii) EPPGE-SWCNT-3PB in 0.1 M pH 7.0 PBS containing 2 x10^{-4} M DA. (b) is the Bodes plot of –phase angle versus logf, and log |Z/Ω| versus logf for the electrodes in (a) above.

8.4. Effect of varying scan rate

The effect of scan rate (25 to 1000 mVs^{-1}) on the electrode kinetics during dopamine oxidation was investigated using the best electrode, EPPGE-SWCNTPABS-3PB. A pair of well-defined redox peaks, with equal peak current heights at all scan rates, was observed (Figure 8.6a). The peak-to-peak separation (ΔE_p) increase from 76 mV at 25 mVs^{-1} to 654 mV at 1000 mVs^{-1}. Deviation of ΔE_p from the ideal 59.8 mV value expected for a one-electron reversible process is indicative of weak electron transfer as the scan rate is increased. The plot of the anodic (I_{pa}) peak current against square root of scan rate ($\nu^{1/2}$) is linear (Figure 8.6b), indicative of diffusion-controlled reaction.

Further, the catalytic reaction kinetic using the RDE technique was explored. Figure 8.6c represents the RDE voltammograms obtained at different rotating speed (ω) for 2 x 10^{-4} M DA electro-oxidation in PBS pH 7.0 using at the EPPGE-SWCNT-3PB. Figure 8.6d is the plot of I_{lim}^{-1} versus $\omega^{-1/2}$ employing the Koutecky-Levich equation below:

$$\frac{1}{i_{\lim}} = \frac{1}{i_k} + \frac{1}{i_{lev}} = \frac{1}{(nFAk_{ch}\Gamma C)} + \frac{1}{(0.620nFAcD^{2/3}\gamma^{-1/6}\omega^{1/2})} \qquad (8.4)$$

where i_{lim}, i_k, i_{lev} are the measured current, kinetic and diffusion-limited currents, respectively, n is the number of electrons transferred which is 2 for DA electrooxidation, k_{ch} is the catalytic rate constant ($mol^{-1}cm^3\ s^{-1}$), F is the Faraday constant (96485 C mol^{-1}), A is the electrode surface area (0.196 cm^2), ω is the rotating speed (rpm), Γ ($molcm^{-2}$) is the redox active species (4.78 x 10^{-8} mol cm^{-2}) concentration on electrode surface, c is the bulk concentration of DA

(2 x 10^{-7} molcm^{-3}), *D* is the diffusion coefficient (cm^{2}s^{-1}) of DA and γ is the kinematic viscosity of the solution.

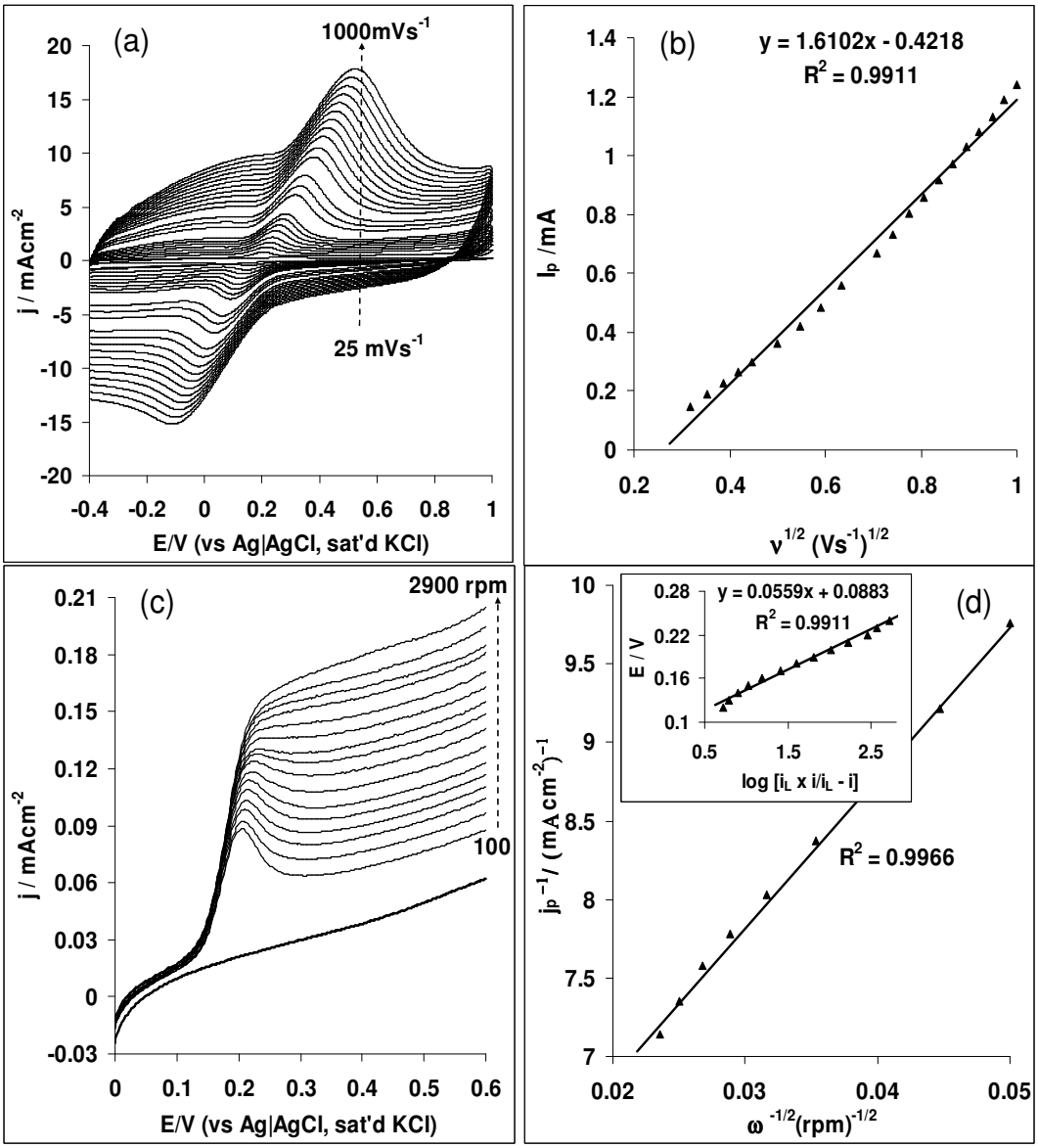

Figure 8.6: (a) Cyclic voltammogram showing the current response of EPPGE-SWCNT-3PB electrodes in 0.1 M PBS solution containing 2x10^{-4} M DA, (b) plot of I_p vs $\nu^{1/2}$ (c) a RDE voltammograms obtained for the EPPGE-SWCNT-3PB in 0.1 M PBS solution containing 2 x 10^{-4} M DA, (d) is the plot of I_p^{-1} vs. $\omega^{-1/2}$. Inset in (d) is the plot of E/V versus log [i x i_L/i_L – i].

The plot is linear with positive intercept, indicating that the electrode reactions are controlled by both kinetics at the electrode surface and the mass transport of DA species. The k_{ch} value obtained from the intercepts of the regression lines was found to be (1.69±0.13)x 10^5 $mol^{-1}cm^3s^{-1}$ (1.69 x 10^2 M^{-1} s^{-1}) which agreed closely with the range of 3.3 x 10^2 to 2.9 x 10^2 M^{-1} s^{-1} for the DA concentration range (5 - 7.5 mM), reported for aluminium electrode modified with nickel pentacyanonitrosylferrate films (NiPCNF/Al) [6]. The difference in the k_{ch} value is due to the catalytic interaction of DA with the different electrode modifier. Correcting the polarization curve for diffusion effects for first order reaction, the Tafel equation may be simplified as Equation 8.5: [7-9].

$$E_{app} = E_{eq} + b\log I_K \tag{8.5}$$

$$I_K = \frac{(i_L.i)}{(i_L - i)} \tag{8.6}$$

$$b = \frac{2.303RT}{\alpha n_\alpha F} \tag{8.7}$$

where E_{app} is the applied potential, E_{eq} is the equilibrium potential, I_k is the kinetic current, i_L is the limiting current (plateau in RDE voltammogram), i is the measured current at a given potential, R, T and F have their usual meaning, αn is the kinetic parameters for the electrode process. At 2500 rpm, the plot of E_{app} versus log I_k (inset in Figure 8.6d) gave Tafel slope of ~ 56 $mVdec^{-1}$ was obtained. The value is closer to the 60 $mVdec^{-1}$ for a fast, one-electron transfer process, followed by a chemical step. An α value close to 1.0 suggest high probability of product formation, meaning an enhanced electrocatalysis [10]. Based on the results, the following reaction

mechanism may be proposed for the electrocatalytic oxidation of DA at the EPPGE-SWCNTPABS-3PB:

$$SWCNT\text{-}PABS/Fe^{3+}/Fe^{2+} \longrightarrow SWCNT\text{-}PABS/Fe^{3+}/Fe^{3+} \quad (8.8)$$

$$SWCNT\text{-}PABS/Fe^{3+}/Fe^{3+} + DA^{+} \longrightarrow SWCNT\text{-}PABS/Fe^{3+}/Fe^{3+}\text{-------}\ DA^{+} \quad (8.9)$$

$$SWCNT\text{-}PABS/Fe^{3+}/Fe^{3+}\text{--------}\ DA^{+} \longrightarrow SWCNT\text{-}PABS/Fe^{3+}/Fe^{2+} + QDA^{+} \quad (8.10)$$

Slow (rate determining step)

$$SWCNT\text{-}PABS/Fe^{3+}/Fe^{3+} + e^{-} \longrightarrow SWCNT\text{-}PABS/Fe^{3+}/Fe^{2+} \quad (8.11)$$

At pH 7, DA (p*Ka* 8.9) exists as a cation with a positively charged amino group [11]. Equation 8.8 represents the catalyst redox pre-equilibrium reaction which shows the electrochemically driven oxidation of the Fe ions in SWCNT-PAB-SO_3^{2-}/$Fe^{3+/}Fe^{2+}$ to SWCNT-PAB-SO_3^{2-}/$Fe^{3+/}Fe^{3+}$. Thereafter, the oxidized catalyst form an adduct with DA. This represents the rate (slow) determining step (rds) (Equation 8.9). Finally, chemical redox process involving oxidation of DA to Dopamine-O-quinone (QDA^{+}) through a two-electron oxidation process occurs (Equation 8.10) and simultaneously, reduction of the oxidized catalyst to the original form takes place. The catalyst is regenerated by the reduction process as represented in Equation 8.11.

8.5. Electroanalysis using square wave voltammetry (SWV), chronoamperometric (CA) and Linear Sweep Voltammetry (LSV).

Concentration study was carried out using different techniques at a fixed potential of 0.20 V exemplified with square wave voltammograms (Figure 8.7a) and the linear sweep voltammogram

(Figure 8.7b). From the plots of current response against concentration, linear relationships (Equations 8.12-8.14) were obtained as:

CA: I_p/μA =(0.16±0.01)[DA]/μM + (3.20±0.01) (R^2 = 0.9999) (8.12)

SWV: I_p/μA =(0.48±0.04)[DA]/μM + (207.25±0.14) (R^2 =0.9996) (8.13)

LSV: I_p/μA = (0.65±0.07) [DA] / μM + (27.78±0.39) (R^2 = 0.9993) (8.14)

The limit of detection (LoD = 3.3 s/m [12]) for the different techniques employed in this study and the linear concentration range are presented in Table 8.2. The analytical values obtained compared favourably and even better than other values reported earlier in the literature for some modified electrodes towards DA detection [13-19]. The re-usability and stability of the EPPGE-SWCNTPABS-3PB were also examined. First, the electrode was repeatedly cycled (50 runs) in pH 7.0 PBS containing 2 x 10^{-4} M DA (not shown). The current decreased from the first scan until about the 30th scan where it then stabilised. However, upon rinsing the electrode in a fresh electrolyte solution and the analysis repeated, about 85% of the initial current height of the DA was obtained, meaning the electrode can be reused after analysis. Similarly, after storage for two weeks in a refrigerator, no significant change in DA current was observed which indicates the electrode stability towards the analyte.

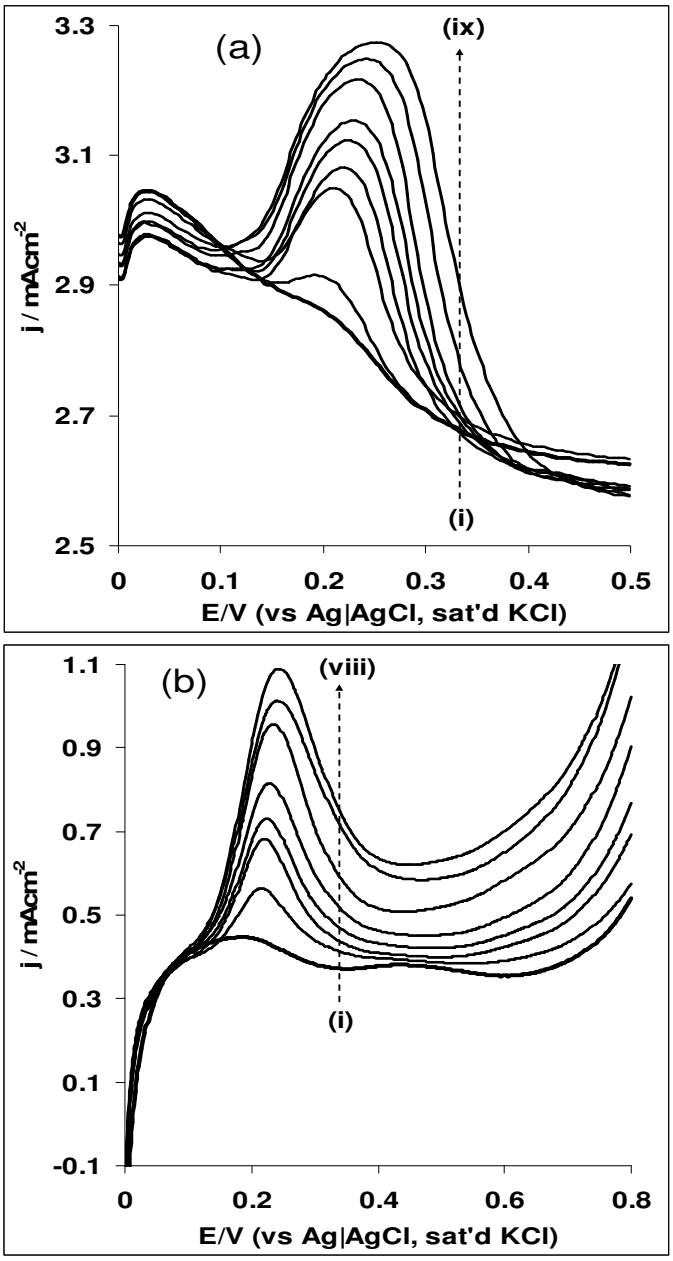

Figure 8.7: (a) Square wave voltammograms evolution of the EPPGE-SWCNT-3PB in 0.1 M PBS solution containing different concentrations of DA (0.0, 6.5, 12.5, 18.2, 23.5, 28.6, 33.3, 42.1 and 50.0 µM (inner to outer; i – ix). (b) Linear sweep voltammogram responses of the EPPGE-SWCNT-3PB in 0.1 M PBS solution containing different concentrations of DA (0.00, 18.2, 28.6, 37.8, 50, 60.5, 66.7, 72.3 µM (inner to outer; i – viii).

Table 8.2: Voltammetric response for dopamine using various modified electrodes.

Electrode	Electrolyte	Method	LCR range (μM)	LoD (μM)	References
EPPGE-SWCNTPABS-3PB	PBS (pH 7.0)	CA	2.4 – 23.1	0.21±0.02	This work
EPPGE-SWCNTPABS-3PB	PBS (pH 7.0)	SWV	6.5 – 50.0	0.92±0.07	This work
EPPGE-SWCNTPABS-3PB	PBS (pH 7.0)	LSV	3.2 – 31.8	1.98±0.16	This work
EPPGE-SWCNT-Fe_2O_3	PBS (pH 7.0)	SWV	0.0 – 31.8	0.36	13
CNT/graphite electrode	PBS (pH 5.0)	DPV	0.5 – 10.0	0.10	14
SDS/MWNTs	PBS (pH 7.4)	DPV	20 – 200.0	3.75	15
CPE-Cobalt salophen	ACS (pH 5.0)	DPV	1.0 – 100.0	0.50	16
PVA modified GCE	PBS (pH 7.0)	DPV	2.0 – 70.0	1.40	17
GCE-PEDOT-PANS	ACS (pH 5.0)	LSV	2.0 – 8.0	0.50	18
GCE/MWCNT-βCD	PBS (pH 7.4)	CR	10.0 – 80.0	6.7	19

SDS: Sodium dodecyl sulfate; **PVA:** Poly(vinyl alcohol); **GCE:** Glassy carbon electrode; **CNT:** Carbon nanotubes; **βCD:** β-cyclodextrin; **CA:** Chronoamperometric; **SWV:** Square wave voltammetry; **DPV:** Differential pulse voltammetry; **LSV:** Linear sweep voltammetry; **PEDOT:**Poly (3,4-ethylenedioxythiophene-co-(5-amino-2-naphthalenesulfonic acid)); **PANS:** Poly 5-amino-2-naphthalenesulfonic acid; **SAM:** Self-assembled monolayer; **PBS:** Phosphate buffer solution; **ACS:** Acetate buffer solution; **LCR:** Linear concentration range; **LoD:** Limit of detection.

8.6. Detection of DA in the presence of AA: Interference study

Figure 8.8 is the cyclic voltammetric responses of EPPGE-SWCNT-3PB electrode in (i) 0.1 M pH 7.0 PBS, (ii) 10 mM AA alone, and mixture of (iii) 9.1 µM DA and 9.1 mM AA, (iv) 16.7 µM DA and 8.3 mM AA, (v) 23.1 µM DA and 7.7 mM AA, (vi) 28.6 µM DA and 7.1 mM AA, (vii) 33.3 µM DA and 6.7 mM AA and (viii) 41.2 µM DA and 5.9 mM AA in PBS pH 7.0. The AA signal which was initially observed at around 0.0 V in the absence of DA remains same after the addition of DA, while the DA signal occurred at around 0.2 V. The results showed that for all the concentrations of the DA studied there was no detectable interference of the AA. Infact, it is interesting to know that DA could be simultaneously detected even at high AA concentration (9.1 mM), which is 1000 times that of DA (9.1 µM), and a potential separation of about 200 mV. The height and amplitude of the peak corresponding to DA also increase proportionally with the DA concentration. On the other hand, at the bare EPPGE (not shown) the AA peaks completely interfere and suppressed the DA signal at around 0.2 V. Indeed, this result is unique when compared to a recent work with Fe_2O_3 nanoparticle that did not allow for the simultaneous detection of DA and AA [13].

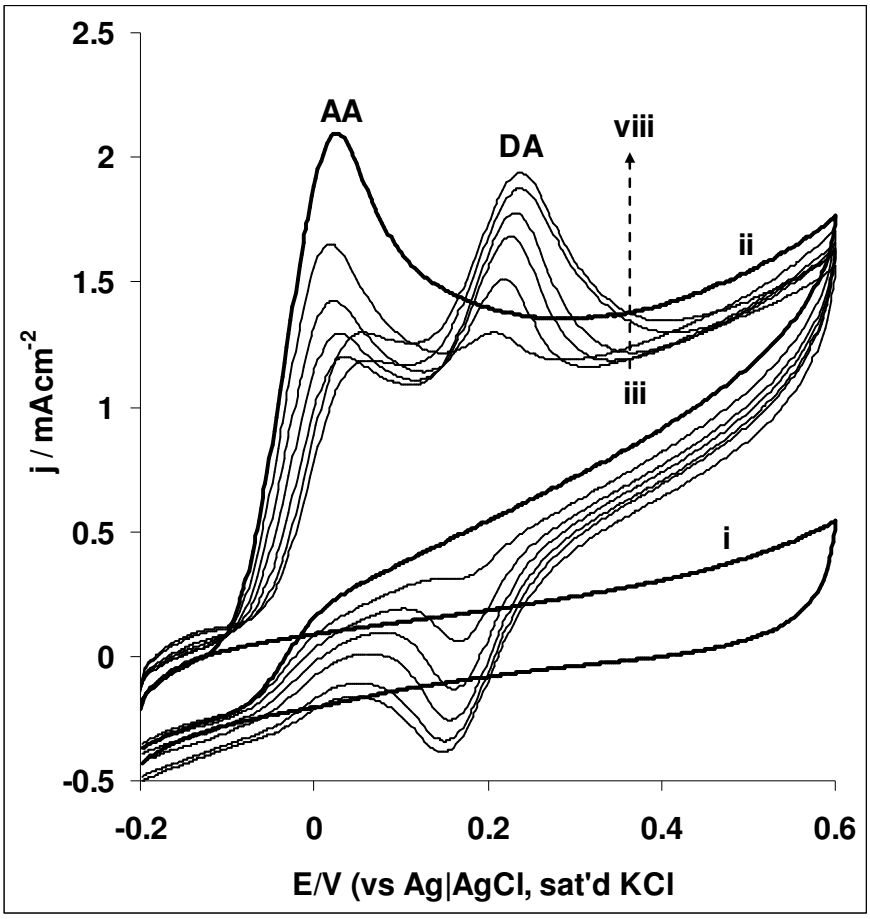

Figure 8.8: Typical square wave voltammograms responses of EPPGE-SWCNT-3PB in (i) 0.1 M pH 7.0 PBS, (ii) 10 mM AA alone, and mixture of (iii) 9.1 µM DA / 9.1 mM AA, (iv) 16.7 µM DA / 8.3 mM AA, (v) 23.1 µM DA / 7.7 mM AA, (vi) 28.6 µM DA/7.1 mM AA, (vii) 33.3 µM DA/6.7 mM AA and (viii) 41.2 µM DA/5.9 mM AA in PBS pH 7.0.

8.7. Real sample analysis: Dopamine drug

To evaluate the potential applicability of the EPPGE-SWCNT-3PB electrode, a square wave voltammetric assay of dopamine present in a dopamine hydrochloride injection, with dopamine content of 200 mg / 5 mL (i.e., 40 mg mL^{-1}) was carried out. The

concentration found in each dopamine drug (Table 8.3) is approximately within the labelled amount, with average recovery (n=5) of 101.60±2.79% at 95% confidence limit. The result further confirms the suitability and reliability of the EPPGE-SWCNT-3PB electrode as a potential sensor for the analysis of neurotransmitter such as DA.

Table 8.3: Determination of dopamine content in dopamine hydrochloride injections (40 mg mL^{-1}), n =5 (at 95% confidence limit) using EPPGE-SWCNT-3PB modified electrode.

Sample	Concentration found/mg mL^{-1}	Recovery/%
1	40.6 ± 0.52	101.5 ± 1.30
3	39.9 ± 1.01	99.8 ± 2.53
4	39.5± 0.96	98.7 ± 2.38
2	40.9 ± 1.24	102.2 ± 3.09

Investigation of the electron transfer behaviour and the catalysis of EPPGE modified with and without SWCNT-PABS/PB nanoparticles towards DA oxidation were carried out. Catalysis of DA was more favoured on the EPPGE-SWCNT-PB in terms of current response and onset potential for catalysis compared with other electrodes investigated. DA response increases with increasing PB layer on the electrode making EPPGE-SWCNT-3PB the best electrode. EPPGE-SWCNT-3PB electrode has the fastest electron transport and lowest R_{ct} towards DA electrocatalysis. The electrode would conveniently detect DA in the presence of AA (1000 times higher) with a wide potential separation of about 200 mV. The electrode is electrochemically stable, re-usable and can be used for the analysis of DA in real drug samples with satisfactory accuracy and reproducibility.

References

1 S. Han, Y. Chen, R. Pang, P. Wan, M. Fan, *Ind. Eng. Chem. Res.* 46 (2007) 6847.

2 L. Wang, S. Guo, X. Hu, S. Dong, *Colld. Surf. A: Physicochem. Eng. Aspects* 317 (2008) 394.

3 Z. Xu, N. Gao, H. Chen, S. Dong, *Langmuir* 21 (2005) 10808.

4 A. Ernst, O. Makowski, B. Kowalewska, K. Miecznikowski, P.J. Kulesza, *Bioelectrochem.* 71 (2007) 23.

5 J. Wang, *Analytical Electrochemistry*, VCH Publisher Inc., New York, 1994, Chapt. 6, p. 171.

6 H. Razmi, M. Agazadeh, B. Habibi-A, *J. Electroanal. Chem.* 547 (2003) 25.

7 A.J. Bard, L.R. Faulkner, *Electrochemical methods-fundamentals and applications*, Wiley, New York 1980.

8 N. Kobayashi, Y. Nishiyama, *J. Phys. Chem.* 89 (1985) 1167.

9 N. Sehlotho, T. Nyokong, *J. Electroanal. Chem.* 595 (2006) 161.

10 J.N. Soderberg, A.C. Co, A.H.C. Sirk, V.I. Birss, *J. Phys. Chem. B.* 110 (2006) 10401.

11 M.J. Giz, B. Duong, N.J. Tao, *J. Electroanal. Chem.* 465 (1999) 72.

12 G.D. Christian, *Analytical Chemistry*, 6th ed. John Wiley and Sons New York, 2004, p113.

13 A.S. Adekunle, B.O. Agboola, J. Pillay, K.I. Ozoemena, *Sens. Actuat. B* 148 (2010) 93.

14 Z. Wang, J. Liu, Q. Liang, Y. Wang, G. Luo, *Analyst* 127 (2002) 653.

15 D. Zheng, J. Ye, W. Zhang, *Electroanalysis* 20 (2008) 1811.

16 S. Shahrokhian, H.R. Zare-Mehrjardi, *Sens. Actuators B Chem.* 121 (2007) 530.

17 Y. Li, X. Lin, *Sens. Actuators B Chem.* 115 (2006) 134.

18 A. Balamurugan, S. Chen, *Bioelectrochem.* 54 (2001) 169.

19 G. Alarco´n-Angeles, B. Pe´rez-Lo´pez, M. Palomar-Pardave, M.T. Ramı´rez-Silva, S. Alegret and A. Merkoci, *Carbon* 46 (2008) 898.